@BoneJointRes

Impact of elevated sclerostin levels on bone resorption

unravelling structural changes and mineral metabolism disruption

From University Hospital Reina Sofia, University of Cordoba, Córdoba, Spain

Cite this article:
Bone Joint Res 2025;14(5):
448–462.

DOI: 10.1302/2046-3758.
145.BJR-2024-0227.R1

Correspondence should be sent to Cristian Rodelo-Haad
crisroha16@gmail.com

M. E. Rodríguez-Ortiz,[1,2] J. M. Díaz-Tocados,[2,3] A. I. Torralbo,[4] K. Valdés-Díaz,[4] A. Rivas-Domínguez,[4] F. Guerrero,[4] I. Reina-Alfonso,[4] M. Naves-Díaz,[2,5] C. Alonso-Montes,[2,5] C. Rodelo-Haad,[1,2] M. Rodríguez,[1,2] J. R. Muñoz-Castañeda,[1,2] IMIBIC Nephrology Group

[1]Nephrology Service, Reina Sofia University Hospital, Maimonides Institute for Research in Biomedicine of Cordoba (IMIBIC), University of Cordoba, Córdoba, Spain
[2]Health Results-Oriented Cooperative Research Network RICORS2040 (Kidney Disease), Institute of Health Carlos III, Madrid, Spain
[3]Vascular and Renal Translational Research Group, Biomedical Research Institute of Lleida, Dr. Pifarré Foundation (IRBLleida), Lleida, Spain
[4]Maimonides Biomedical Research Institute of Cordoba (IMIBIC), University Hospital Reina Sofia, University of Cordoba, Córdoba, Spain
[5]Bone and Mineral Research Unit, Hospital Universitario Central de Asturias, Instituto de Investigación Sanitaria del Principado de Asturias (ISPA), Oviedo, Spain

Aims

The physiological function of sclerostin remains unknown. Sclerostin is synthesized by osteocytes and operates by inhibiting the Wnt/β-catenin pathway. Similarly, it is well established that low levels of sclerostin lead to enhanced bone formation and reduced calciuria, and that high levels of sclerostin are associated with osteoporosis.

Methods

The impact of high levels of recombinant sclerostin on bone and mineral metabolism parameters was analyzed in this study. In male healthy rats, the effects of three elevated doses of sclerostin over a 14-day period were studied, involving bone histomorphometry, micro-CT (μCT), immunohistochemistry, and analysis of mineral metabolism parameters.

Results

Although there was increased bone formation, high doses of sclerostin led to a higher reduction in trabecular bone volume due to a significant increase in bone resorption through the direct activation of osteoclastogenesis. In vitro, sclerostin promoted the differentiation of bone marrow stem cells into osteoclasts. Bone resorption, as measured by tartrate-resistant acid phosphatase (TRAP) activity, was excessive in trabecular, cortical, and subchondral bone. Similarly, high doses of sclerostin increased the number of hypertrophic chondrocytes, consequently expanding the growth plate area. At the cortical level, positive TRAP staining could be observed, suggestive of osteocytic osteolysis and trabecularization of cortical bone. The increased bone resorption resulted in a substantial rise in the urinary excretion of phosphorus and calcium, accompanied by elevated levels of FGF23 and a significant decrease in parathyroid hormone (PTH).

Conclusion

These findings suggest that elevated levels of sclerostin promote bone resorption through the activation of osteoclasts and the generation of osteocytic osteolysis, resulting in increased calciuria, phosphaturia, and changes in mineral metabolism.

Bone & Joint Research

Article focus

- The impact of reduced or absent sclerostin levels on increased cortical bone and decreased calciuria has been well documented. However, the effects of elevated sclerostin levels on bone changes and mineral metabolism remain underexplored.
- Further investigation into the impact of high sclerostin levels on bone and mineral metabolism is essential to better understand the skeletal changes that occur in conditions characterized by elevated sclerostin, such as chronic kidney disease.

Key messages

- High doses of sclerostin increase bone resorption, alter osseous microarchitecture, and promote osteoclastogenesis.
- Sclerostin also induces trabecularization of cortical bone, triggering the development of osteocytic osteolysis.
- Elevated sclerostin induces changes in urinary calcium and phosphorus, as well as in the circulating levels of parathyroid hormone (PTH) and FGF23, thus revealing a new key element in mineral homeostasis.

Strengths and limitations

- Our work involves the use of an in vivo experimental model that resembles the effect of a chronic and continuous administration of sclerostin. The findings that are shown in the article are novel and interesting, showing that high sclerostin markedly alters bone structure. All together, these results suggest that the elevated concentrations of sclerostin that are normally found in chronic kidney disease patients might contribute to renal osteodistrophy.
- This work only involved the use of male rats. Therefore, sex-related differential effects of sclerostin cannot be ruled out.

Introduction

Sclerostin, a protein encoded by the SOST gene, is pivotal in bone metabolism. Predominantly synthesized by osteocytes, it serves as a key negative regulator of bone formation by binding to transmembrane proteins LRP5/6, facilitating the degradation of β-catenin.[1] The understanding of the functions of sclerostin is still limited. Research utilizing SOST-KO mice has revealed an aberrant activation of Wnt/β-catenin signalling, leading to heightened bone formation and increased cortical bone density.

However, in the clinical scenario, it is more common to find elevated rather than low sclerostin levels, as in chronic kidney disease (CKD) patients.[2,3] In fact, in advanced stages of CKD, a relationship between high sclerostin levels and cardiovascular mortality has been reported.[4] The reasons for an increase of sclerostin levels in CKD patients are not clear.

It is known that bone sclerostin expression is reduced in response to parathyroid hormone (PTH) in vitro and in vivo.[5] Along the same line, other studies have proposed that the decrease in PTH levels is associated with an increase in sclerostin.[6] Furthermore, in peritoneal dialysis patients, it has been suggested that the PTH/sclerostin ratio may serve as a more reliable marker of low bone turnover than PTH levels alone;[7] thus, sclerostin plays an important role in the regulation of mineral metabolism. However, presently, it is not clear how sclerostin interacts with other elements of mineral metabolism.

There is not much information about the consequences of high or physiological levels of sclerostin on bone, and how it affects other parameters of mineral metabolism. The present study aimed to shed light on the physiological impact of sclerostin on trabecular, cortical, and subchondral bone. To accomplish this goal, we used an experimental rat model involving the continuous infusion of high levels of recombinant sclerostin. Additionally, the relationship between sclerostin levels and other parameters of mineral metabolism was explored in this setting.

Methods

Animals

Healthy male Wistar rats (Charles River Laboratories, USA), aged nine to ten weeks and weighing 250 to 300 g, were individually housed using a 12-hour/12-hour light/dark cycle. Animals were given ad libitum access to a standard diet (Altromin, Germany). Ethical approval was obtained from the Ethics Committee for Animal Research of the University of Cordoba and Junta de Andalucia. Animals received humane care in compliance with the Principles of Laboratory Animal Care from the National Society for Medical Research.[8] An ARRIVE checklist is included in the Supplementary Material to show that the ARRIVE guidelines were adhered to in this study.

A total of 20 rats were randomly allocated into four experimental groups receiving either vehicle or 750, 1,500, or 3,000 pg/ml of recombinant sclerostin per day. Initially, five animals were planned for each group. During the experiment, some animals were excluded due to technical issues related to pump implantation. As a result, the final number of animals per group was as follows: vehicle (n = 4), SOST 750 pg/ml (n = 4), SOST 1,500 pg/ml (n = 4), and SOST 3,000 pg/ml (n = 6). These numbers were sufficient to detect statistically significant differences among the groups. No inclusion criteria were adopted during the experiment; animals in which implantation errors due to human handling were identified were excluded from the final analyses, and there were no other exclusion criteria. In this sense, we retrieved the first round of animals corresponding to each group (one per group) due to human failure to implant the correct Alzet pump model. For this reason, these animals were discarded from the experiment. Finally, two rats in the group with the highest dose of sclerostin (3,000 pg/ml) were added.

Alzet pumps (model 2002; ALZET, USA) were filled in aseptic conditions with recombinant rat sclerostin (Cusabio, USA) diluted in 10 mM Tris-HCl pH 8.0 buffer, providing constant sclerostin infusion for 14 days. Considering a blood volume of 60 ml/kg and aiming to achieve plasma concentrations of sclerostin at 750, 1,500, and 3,000 pg/ml, daily infusions of 12 µl were administered at concentrations of 1.075 ng/ml, 2.15 ng/ml, and 4.3 ng/ml, respectively. Pumps were implanted subcutaneously between the shoulders. Mineralization was evaluated through double labelling by subcutaneous calcein (Sigma-Aldrich, USA) administration (25 mg/kg) to the rats, two and nine days before kill. Rats were housed in metabolic cages to collect 24-hour urine samples before kill on day 14 of the experiment. Potential confounders such as the order of treatments and measurements, or animal/cage location were not controlled. The first author

of the study (MERO) was aware of the group allocation at different stages of the experiment and during the subsequent data analysis. Euthanasia was performed by aortic puncture and exsanguination under general anaesthesia with sevoflurane. Blood samples were collected in heparinized syringes from the abdominal aorta. Afterwards, plasma was separated by centrifugation and stored at -80°C until use. The organs of interest were collected for subsequent processing.

Bone histomorphometry

At euthanization, right femora were dissected and placed in 70% ethanol. The femora were dehydrated in alcohol, treated with xylene, and embedded in 75% methyl methacrylate, 25% dibutyl phthalate, and 2.5% w/v benzoyl peroxide. Histomorphometric parameters were evaluated in undecalcified 5 mm sections of the distal bone stained with modified Masson-Goldner trichrome technique. Briefly, slices were fixed with 50% ethanol with pressure, rehydrated and stained with haematoxylin-ferric chloride 1:1, then cleared with 1% hydrogen chloride (HCl) and turned blue with lithium carbonate ($LiCO_3$). After being rinsed with water, slices were stained with Goldner's trichrome dye for 20 minutes and then rinsed with 1% acetic acid. Subsequently, samples were stained with safranin for five minutes, dehydrated with ethanol, and mounted. Green-stained areas were considered mineralized bone and red-stained areas measuring at least 1.5 mm were identified as osteoid.

Bone histomorphometry parameters were assessed in cancellous bone within the secondary spongiosa (at a distance of 0.25 mm from the endocortical bone and the growth plate) under 200× magnification, using OsteoMeasure software (OsteoMetrics, USA), and derived indices were determined by standard calculations.[9] Bone dynamic parameters were calculated by the measurement of the single and double fluorescent calcein labelling lines in undecalcified 10 mm serial sections.

Micro-CT analyses

For micro-CT (μCT) analysis, rat femora were scanned using a Bruker 1176 microCT device (50 kV, 500 μA) (Bruker, USA) with a 1,000 × 668 matrix, 35 mm field of view, 0.5 mm aluminium filter, and 0.5° rotation angle. Images were reconstructed using NRecon (Micro Photonics, USA) to correct beam-hardening and ring artifacts. Trabecular and cortical bones were segmented and analyzed separately: trabecular bone analyses were performed at a 5 mm distance from the distal femur with a length of 2.5 mm, while cortical analysis included slices spanning 1.5 mm at the mid-diaphysis. Using Bruker CTAn software (Bruker), trabecular parameters (bone volume fraction (BV/TV), trabecular thickness (Tb.Th), trabecular separation (Tb.Sp), number of trabeculae (Tb.N)), and cortical parameters (bone area, thickness, bone mineral density (BMD)) were quantified. 3D Slicer software (version 5.2.1) was used for 3D visualization, and to provide representative images across experimental groups.[10]

Immunohistochemistry

Left femora were fixed in 4% formalin and embedded in paraffin after decalcification with ethylenediaminetetraacetic acid (EDTA) 10% pH 7.4 for 28 days and 4°C. Next, 4 mm sections were deparaffinized in xylene and rehydrated in ethanol. Immunostaining was performed by using the ImmPRESS HPR Universal and Polymer kit (Vector Laboratories, USA). Sections were incubated overnight at 4°C with a mouse anti-β-catenin antibody (1:50 dilution; BD Bioscences, USA). Sections were counterstained with haematoxylin for 30 seconds (PanReac AppliChem; ITW Reagents, Germany) and dehydrated. Staining with only polymer without primary antibody was used as a negative control to avoid unspecific signals.

TRAP staining

Tartrate-resistant acid phosphatase (TRAP) staining was performed after bone decalcification with 10% EDTA for 28 days. The bones were later dehydrated and embedded in paraffin. TRAP staining was evaluated separately in trabecular, cortical, and subchondral bone.

Briefly, slices were incubated in basic solution containing sodium acetate anhydrous, L-(+)-tartaric acid, glacial acetic acid, and distilled water for 30 minutes and 37°C to reduce noise. Later, Naphthol AS-BI substrate solution was included, and the slices were incubated for 30 additional minutes. The following step was to mix sodium nitrate solution and pararosaniline dye for 30 seconds and to add basic solution, and it was incubated for seven minutes and washed with distilled water. Finally, bone slices were stained with Carazzi's haematoxylin for one minute and washed again with water, then mounting medium was added. Pink areas with cells containing two or more nuclei were considered as osteoclastic cells. Images were obtained with a Leica DM 2000 and a Camera Leica MC190 HD (Leica, UK).

Osteoclast differentiation from rat bone marrow stem cells

Six male Wistar rats, each weighing approximately 250 g, were anaesthetized with sevoflurane and euthanized by aortic puncture. Femora and tibiae were collected, and bone marrow was perfused as follows: bones were dissected at the epiphyses and subsequently perfused with α modification-minimal essential medium (αMEM; Sigma-Aldrich) containing 15% fetal bovine serum (FBS; Lonza, USA), 1% ultra-glutamine (Lonza), 100 U/ml penicillin, and 100 μg/ml streptomycin. A single-cell suspension was obtained by filtration through a 70 μm cell strainer (BD Biosciences). The cells were then centrifuged and suspended in ammonium-chloride-potassium (ACK) lysing buffer. Cells were subsequently centrifuged and cultured in α-MEM supplemented with 10% FBS and 10 ng/ml rat recombinant M-CSF (PeproTech; Thermo Fisher Scientific, USA), and maintained at 37°C with 5% CO_2 and saturated humidity. After 24 hours, non-adherent cells were collected and cultured in six-well plates with α-MEM supplemented with 10% FBS and 30 ng/ml rat recombinant M-CSF and incubated in the same conditions. After three days, adherent cells were carefully harvested using a scraper, counted in a Neubauer chamber, and then cultured in 24-well plates with α-MEM containing 10% FBS, 30 ng/ml rat recombinant M-CSF, and 100 ng/ml rat recombinant receptor activator of NF-κB ligand (RANKL). At this point, either 1 ng/ml of sclerostin or vehicle was added. The culture medium was replaced every two days, and after five days the cells were processed to quantify the expression of cathepsin K (CTSK) messenger RNA (mRNA) and subjected to TRAP staining, both of which are commonly used as markers for osteoclast markers.

Identification of TRAP-positive cells

TRAP staining was carried out using a commercially available Leukocyte Acid Phosphatase (TRAP) Kit from Sigma-Aldrich, following the manufacturer's instructions. In brief, cells were fixed with a citrate-paraformaldehyde-acetone solution for 30 seconds at room temperature, washed three times with deionized distilled water (ddH2O) pre-warmed to 37°C, and then incubated in a TRAP-staining solution (comprising 0.25 M acetate, 0.7 mg/ml diazotized Fast Garnet GBC, 1.25 mg/ml Naphtol AS-BI phosphate, and 0.67 M tartrate) at 37°C for one hour. Subsequently, the cells were washed twice with ddH_2O, counterstained with haematoxylin for two minutes, rinsed with tap water, and air-dried. Microphotographs were taken using a Leica DM2000 LED microscope (Leica).

RNA isolation and RT-PCR

Total RNA was extracted with 1 ml of TRI reagent (Sigma-Aldrich) following a modification of the Chomczynski and Sacchi protocol,[11] and quantified by spectrophotometry (ND-1000; NanoDrop Technologies, USA). Isolated RNA samples were treated with DNase amplification grade (Sigma-Aldrich), following manufacturer instructions. Real-time PCR was assayed with 50 ng of treated RNA using SensiFAST SYBR No-ROX One-Step Kit (Bioline, UK) in a final volume of 20 µl following manufacturer instructions. Primers from cathepsin K and glyceraldehyde-3-phosphate dehydrogenase (GAPDH) (purchased from Eurofins Genomics, Germany) used for real-time reverse transcription polymerase chain reaction (RT-PCR) were the following: cathepsin K (forward 5'TCTCTGTACCCTCTG-CACTTAG3'; reverse 5'ATTGAC TCTGAAGACGCTTACC3') and GAPDH (forward 5'AGGGCTGCC TTCTCTTGTGAC3'; reverse 5'TGGGTAGAATCA-TACTGGAACATG TAG3'). PCR amplification was performed using LightCycler 480 (Roche Molecular Biochemicals, USA). The expression of cathepsin K was normalized according to that of GAPDH. The formula $2^{-\Delta\Delta CT}$ was used to show the relative expression of cathepsin K as fold change.

Serum and urine biochemistries

Serum and urine total calcium, phosphorus, and creatinine were determined by spectrophotometry (BioSystems, Spain). Enzyme-linked immunosorbent assay (ELISA) kits were used for the measurement of intact FGF23 (KAINOS Laboratories, Japan), c-terminal FGF23 (QuidelOrtho, USA), and intact PTH (QuidelOrtho). In urine, the C-telopeptides of cross-links of type I collagen (CTx) levels were determined using CrossLaps ELISA (IDS, USA).

Statistical analysis

Values are expressed as means and SDs. The differences between means for either two different groups, or more than two different groups, were assessed by independent-samples *t*-test or two-way analysis of variance (ANOVA), respectively, or the corresponding non-parametric test. ANOVA was followed by post hoc Fisher's least significant difference post hoc test. A linear regression or curve fitting test was used to assess the correlation between two variables. A p-value lower than 0.05 was considered statistically significant.

Results

The administration of sclerostin during a 14-day period increased β-catenin degradation in bone cells

The effect of sclerostin on β-catenin degradation in bone cells was evaluated after the continuous subcutaneous infusion of either vehicle (Veh) or sclerostin to rats at doses of 750, 1,500, and 3,000 pg/ml. The data obtained are shown in Supplementary Figures a, ba, and bb. The immunohistochemistry shows that the administration of sclerostin induced a substantial decrease in β-catenin content in bone cells, particularly in hypertrophic and calcified chondrocytes, as well as in osteoblasts in the trabecular bone.

Changes in rat trabecular and cortical bone after 14 days administration of sclerostin

µCT analysis, shown in Figure 1a, clearly demonstrates a substantial loss of bone density following the administration of any of the doses of sclerostin. Figures 1b to 1e show the changes in TRAP activity in the different experimental groups. In the trabecular bone, it was evident that, compared with the vehicle group, high concentrations of sclerostin led to a substantial increase in the number of osteoclasts, which resulted in a higher resorptive activity in the trabecular bone. Supplementary Figure bc shows the quantification of the number of TRAP-positive cells in the trabecular bone. Significant increases in TRAP activity were observed following the administration of sclerostin.

Representative microphotographs of trabecular bone stained with Goldner's trichrome are shown in Supplementary Figure c. Bone histomorphometric analyses performed in femora showed that the administration of any of the high doses of sclerostin resulted in a significant reduction in bone volume (Figure 2a), accompanied by a substantial increase in bone turnover. Osteoid volume was increased along with a rise in the osteoblast surface (Figures 2b to 2d). In addition, it is important to note that parameters associated with bone resorption, including eroded surface, osteoclast surface, and number of osteoclasts (Figures 2e to 2h) also exhibited significant increases after continuous sclerostin administration. This elevated resorptive activity resulted in a reduction in bone volume. This increased resorptive activity induced by sclerostin had a marked impact on bone trabecular microstructure. In these rats, there was a greater separation between trabeculae, which were also thinner (Figures 2i to 2k), although the number of trabeculae did not change significantly.

Changes in the cortical bone after administration of recombinant sclerostin for 14 days in rats

To assess the sclerostin-induced changes at cortical level, we performed studies using µCT. In Figure 3a, cross-sectional slices of cortical femora from each group (vehicle, 750 pg/ml, 1,500 pg/ml, and 3,000 pg/ml) illustrate a reduction in the mineralized area and thinner cortical bone. These changes were quantified by measuring cortical volume (Figure 3b), cortical area (Figure 3c), and cortical porosity (Figure 3d). Both cortical volume and area exhibited significant decreases after the administration of the different doses of sclerostin. The difference in the cortical area was only statistically significant with the dose of 1,500 pg/ml ($p = 0.034$ vs Veh group, one-way ANOVA).

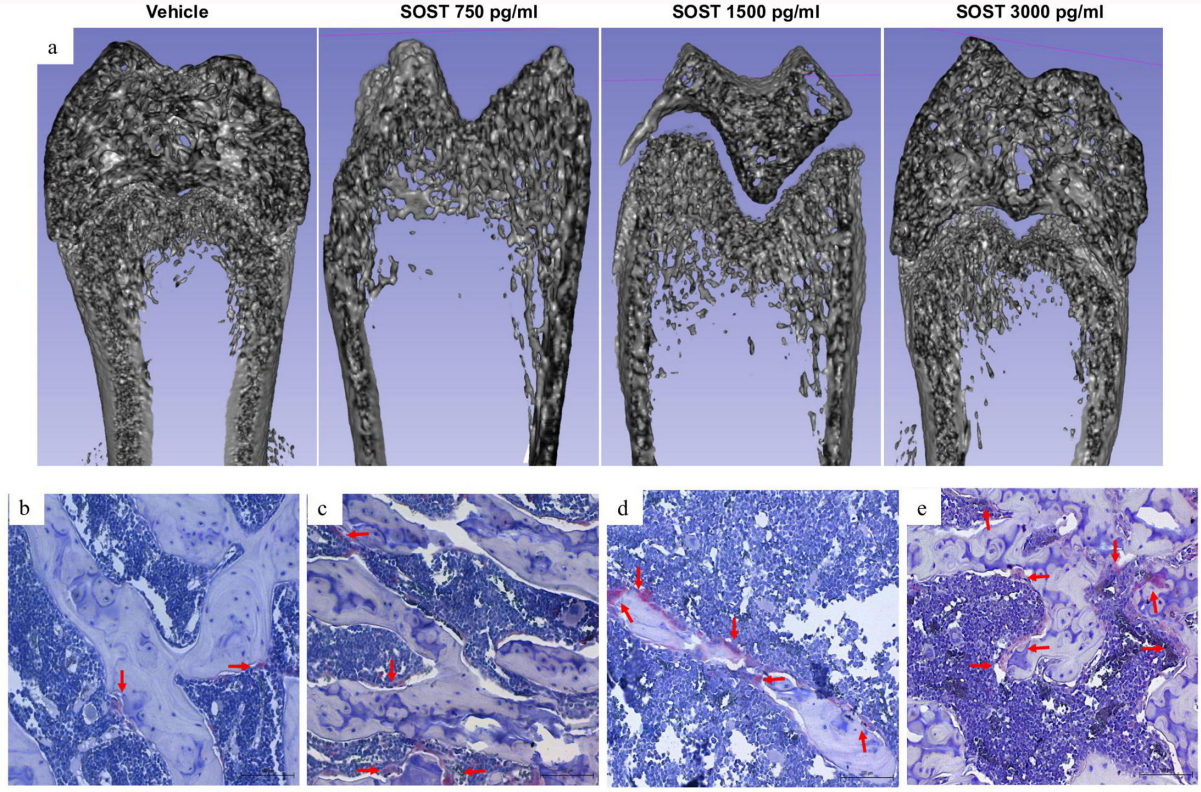

Fig. 1

High levels of sclerostin promote bone trabecular resorption. a) Micro-CT (μCT) analysis revealed a significant reduction in trabecular bone volume. Images generated using 3D Slicer software illustrated a decrease in trabecular bone volume in all rats receiving sclerostin. Representative images obtained from 3D Slicer software are provided for each experimental group. b) Tartrate-resistant acid phosphatase (TRAP) staining was performed to evaluate trabecular bone resorption. In comparison with the b) vehicle group, the number of osteoclasts in trabecular bone, identified by their red staining (red arrows) and the presence of two or more nuclei, showed a significant increase after the administration of recombinant sclerostin at doses of c) 750, d) 1,500, and e) 3,000 pg/ml (n = 5 animals per group). Figure 200× magnification. Scale bar: 100 μm.

The impact of recombinant sclerostin on cortical bone was further investigated using Goldner's trichrome staining (Figures 3d to 3g) and TRAP staining (Figures 4a to 4d). Compared with the vehicle group, the administration of sclerostin increased cortical porosity and fibrosis while decreasing mineralization. This bone histomorphometry study suggests a trabecularization of cortical bone (Figures 3d to 3g) similar to what is observed with ageing.[12] TRAP staining (Figures 4a to 4d) revealed the presence of positive TRAP activity in some osteocytes and around the periosteum, which suggests osteocytic osteolysis. Supplementary Figure bd shows the quantification of the number of TRAP-positive cells in the cortical bone. A significant increase in TRAP activity ($p < 0.050$ vs vehicle group, one-way ANOVA) was observed in all animals treated with recombinant sclerostin.

High levels of recombinant sclerostin promote osteoclastogenesis of rat bone marrow mononuclear cells

To provide a clearer understanding of the effect of sclerostin on osteoclasts, additional experiments were conducted in osteoclasts differentiated from rat bone marrow mononuclear cells, both in the presence and absence of recombinant sclerostin (1 ng/ml). The progressive changes observed from undifferentiated cells to differentiated osteoclasts are illustrated in Figures 4e to 4h. In these differentiated cells, there was an increase in TRAP staining (Figures 4e to 4g) and higher mRNA cathepsin K expression (Figure 4h). Remarkably, during the differentiation process, the addition of sclerostin led to a significant increase in cathepsin K expression along with the formation of very large osteoclasts with more intense TRAP staining.

Changes in growth plate induced by sclerostin

Recombinant sclerostin administration had additional effects on bone structure, particularly within the growth plate. As depicted in Figures 5a to 5d, the growth plate in sclerostin-treated animals exhibited increased width and contained a greater number of proliferative and hypertrophic chondrocytes.

Histomorphometric analyses revealed a notable increase in the cell count within the growth plate following sclerostin administration (Figure 5e). Furthermore, these chondrocytes exhibited a significant increase in size, as indicated in Figure 5f. This combined effect of enhanced chondrocyte size and number contributed to a substantial expansion of the total growth plate area, as shown in Figure 5g.

Intriguingly, TRAP staining yielded positive results in osteoclast precursors located within adjacent sinusoids in the calcification areas of the metaphysis (Figures 5h to 5k). Again, there were no significant differences between the doses of sclerostin. Supplementary Figure be shows the number of TRAP-positive cells in the subchondral bone. A significant increase in TRAP activity was observed in animals treated with

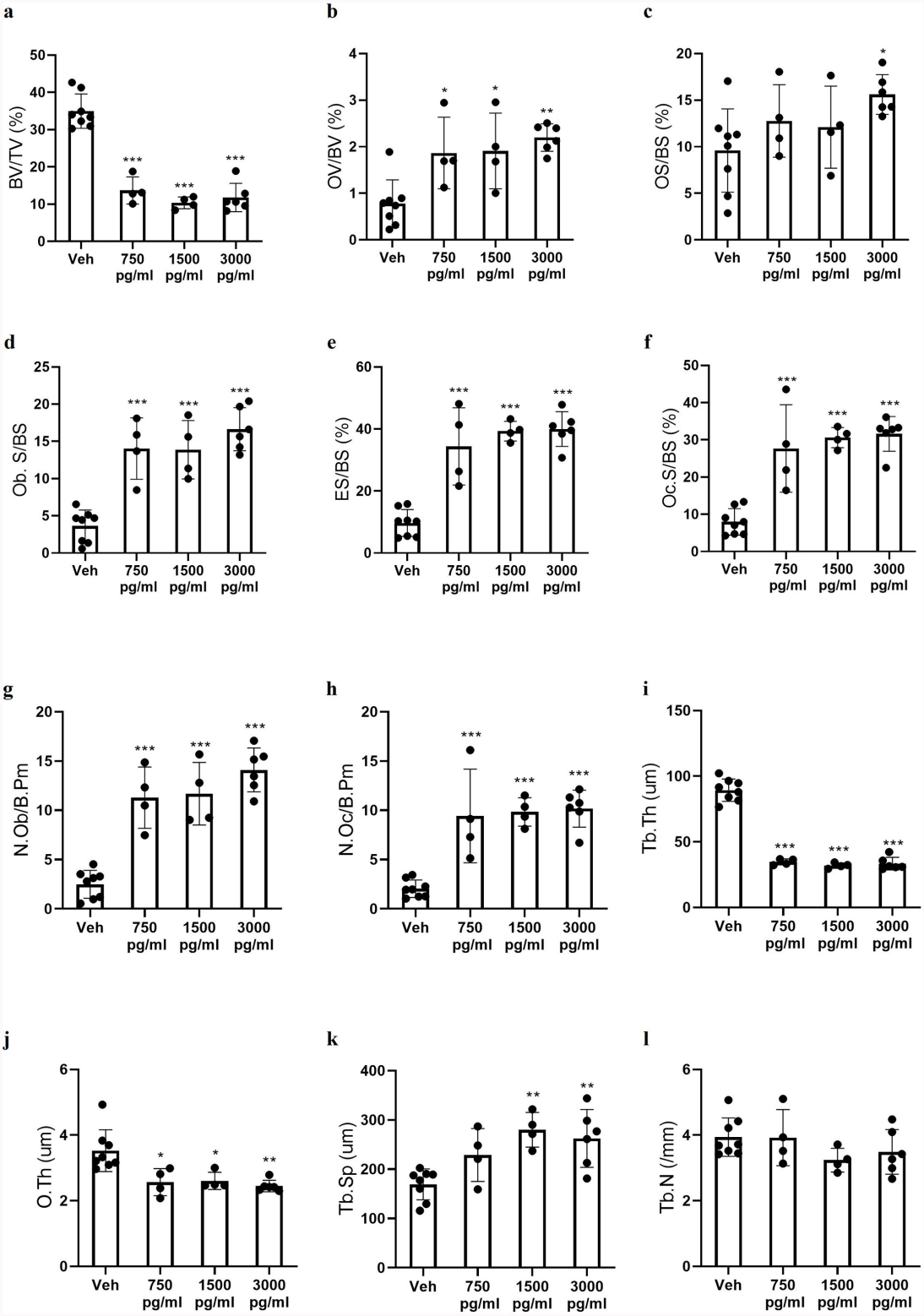

Fig. 2

Effects of recombinant sclerostin infusion in bone histomorphometric parameters of trabecular bone. The administration of different doses of recombinant sclerostin induced a reduction in a) bone volume fraction (BV/TV), and an increase of bone turnover measured by b) an augment of osteoid volume (OV/BV), c) osteoid surface (OS/BS), d) osteoblast surface (Ob.S/BS), e) eroded surface (ES/BS), f) osteoclast surface (Oc.S/BS), g) number of osteoblasts (N.Ob/B.Pm), and h) number of osteoclasts (N.Oc/B.Pm). Parameters of bone microarchitecture were also modified to the same extent by the different doses of sclerostin. i) Trabecular thickness (Tb.Th) and j) osteoid thickness (O.Th) decreased significantly compared with the vehicle (Veh) group after sclerostin infusion. Finally, the highest doses of sclerostin (1,500 and 3,000 pg/ml) increased k) trabecular separation (Tb.Sp), while the i) number of trabeculae (Tb.N) was not modified following sclerostin infusion. n = 4 for Veh, SOST 750, and SOST 1,500 pg/ml groups, and n = 6 for SOST 3,000 pg/ml. *p < 0.05; **p < 0.01, ***p < 0.001 versus Veh group (two-way analysis of variance with Fisher's least significant difference post hoc test).

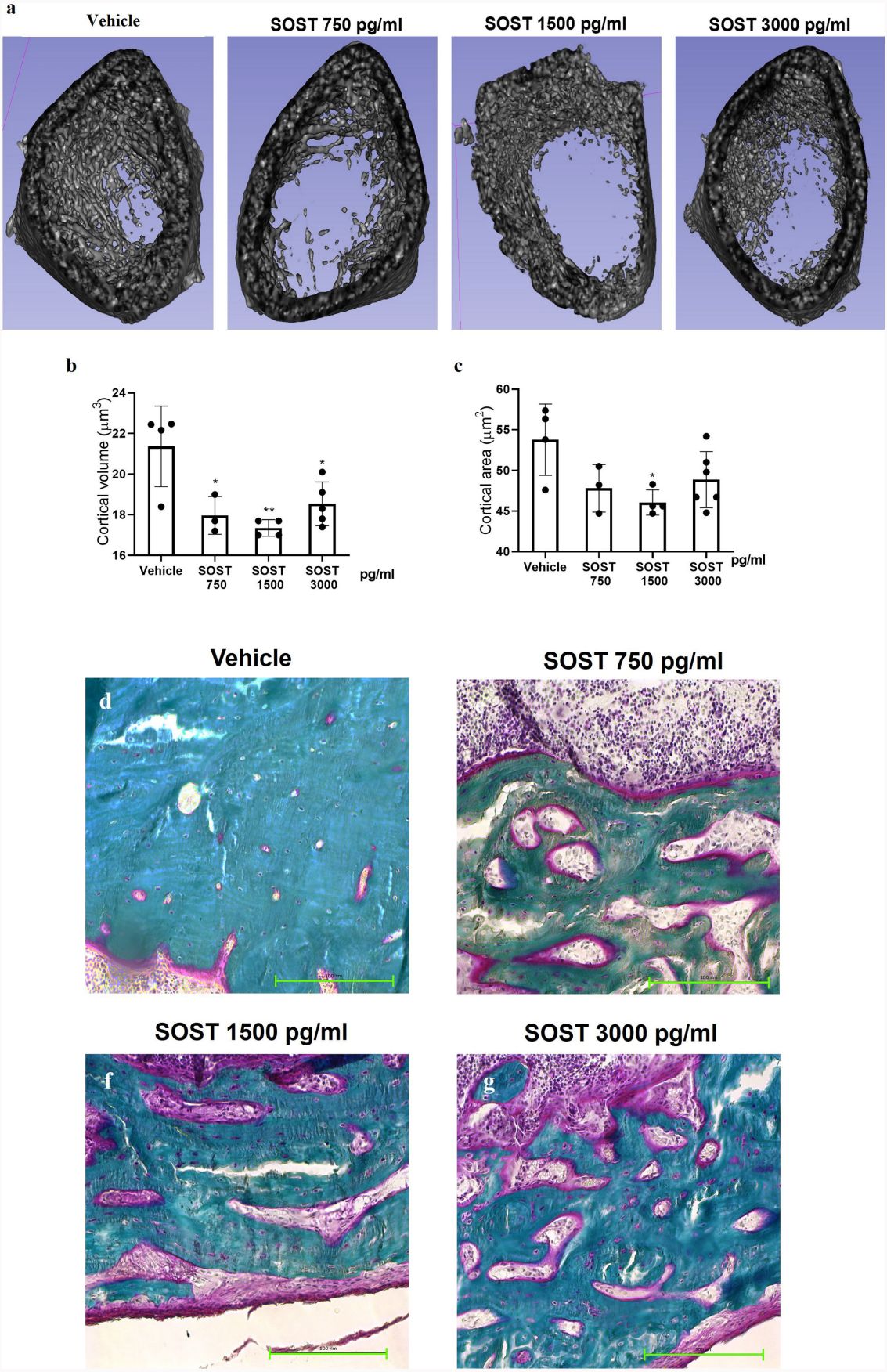

Fig. 3

Sclerostin infusion yields more porosity and trabecularization of cortical bone. a) Images generated using 3D Slicer software illustrated a decrease in the cortical volume with all doses of sclerostin. Representative images are provided for each experimental group. b) Compared with the vehicle group, the cortical volume was significantly reduced with any dose of sclerostin. c) However, the cortical area had a clear tendency to decrease, although only the dose of 1,500 pg/ml of sclerostin showed statistically significant changes. d) to g) Representative images of cortical trabecular status by Goldner's trichrome staining in d) the vehicle group, e) 750 pg/ml, f) 1,500 pg/ml, and g) 3,000 pg/ml of sclerostin are shown (n = 4 for vehicle, SOST 750, and SOST 1,500 pg/ml groups, and n = 6 for SOST 3,000 pg/ml). Figure 200× magnification. Scale bar: 100 μm. *p < 0.05, **p < 0.01 versus vehicle group (two-way analysis of variance with Fisher's least significant difference post hoc test).

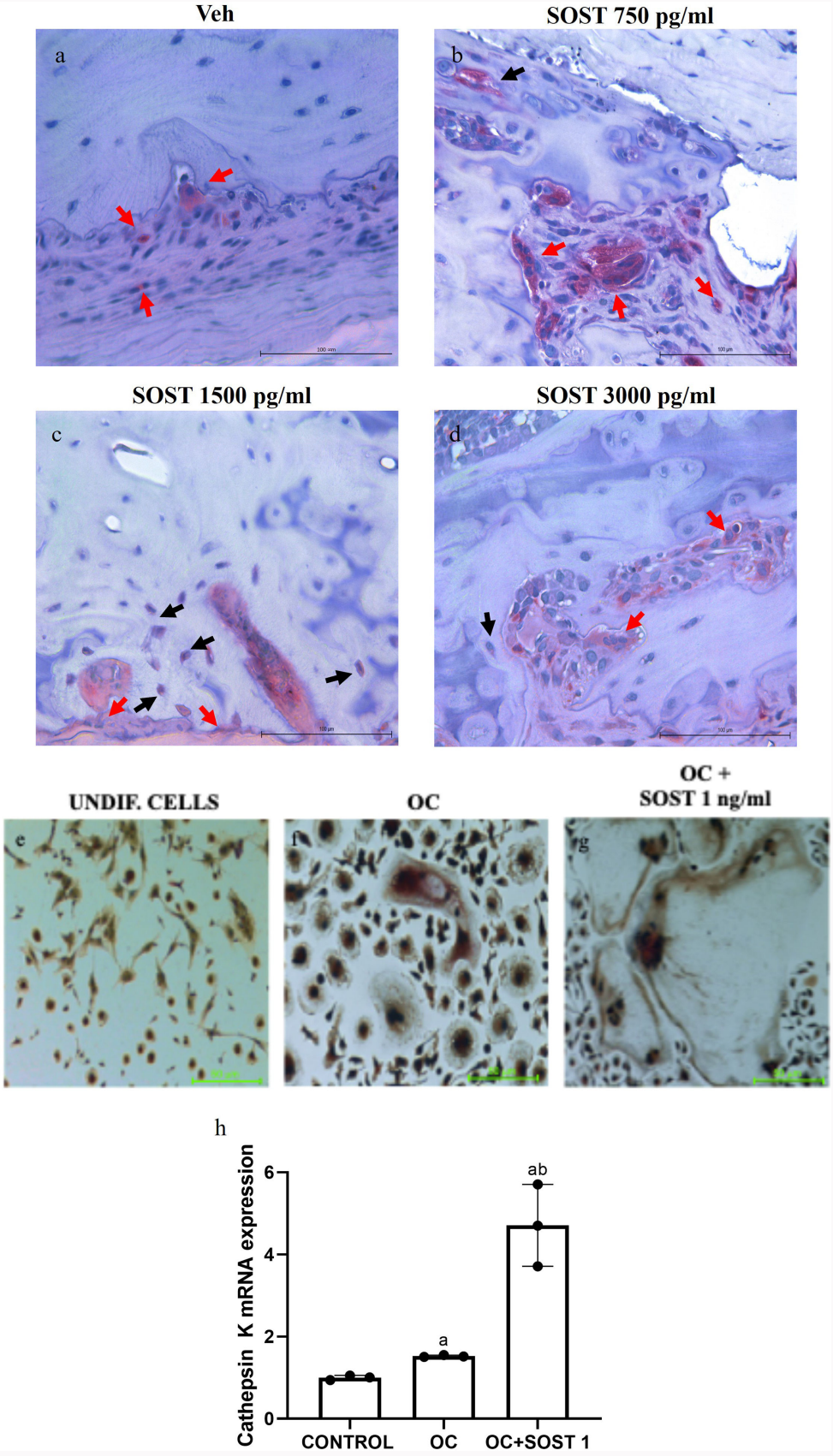

Fig. 4

The impact of high sclerostin levels on the activation of cortical bone resorption promoting osteoclastogenesis. Compared with a) the vehicle (Veh) group, the number of osteoclasts in cortical bone and periosteum, identified by their red staining (red arrows) and by containing two or more nuclei, were significantly increased in rats receiving sclerostin at doses of b) 750, c) 1,500, or d) 3,000 pg/ml (n = 4 for Veh, SOST 750, and SOST 1,500 pg/ml groups, and n = 6 for SOST 3,000 pg/ml). Figure 200× magnification. Scale bar: 100 μm. The administration of sclerostin promoted osteoclastogenesis of rat bone marrow stem cells. Tartrate-resistant acid phosphatase (TRAP) staining was performed in e) undifferentiated (Undif.) cells (UC), f) osteoblasts differentiated from bone marrow stem cells (OC), and g) differentiated osteoclasts treated with sclerostin at a dose of 1 ng/ml (OC + SOST). h) The messenger RNA (mRNA) expression of cathepsin K increased after osteoclast differentiation, and the addition of 1 ng/ml of sclerostin during osteoclast differentiation resulted in a marked increase in the expression of cathepsin K mRNA ([a]$p < 0.05$ vs undifferentiated cells (control, independent-samples *t*-test); [b] $p < 0.05$ vs OC).

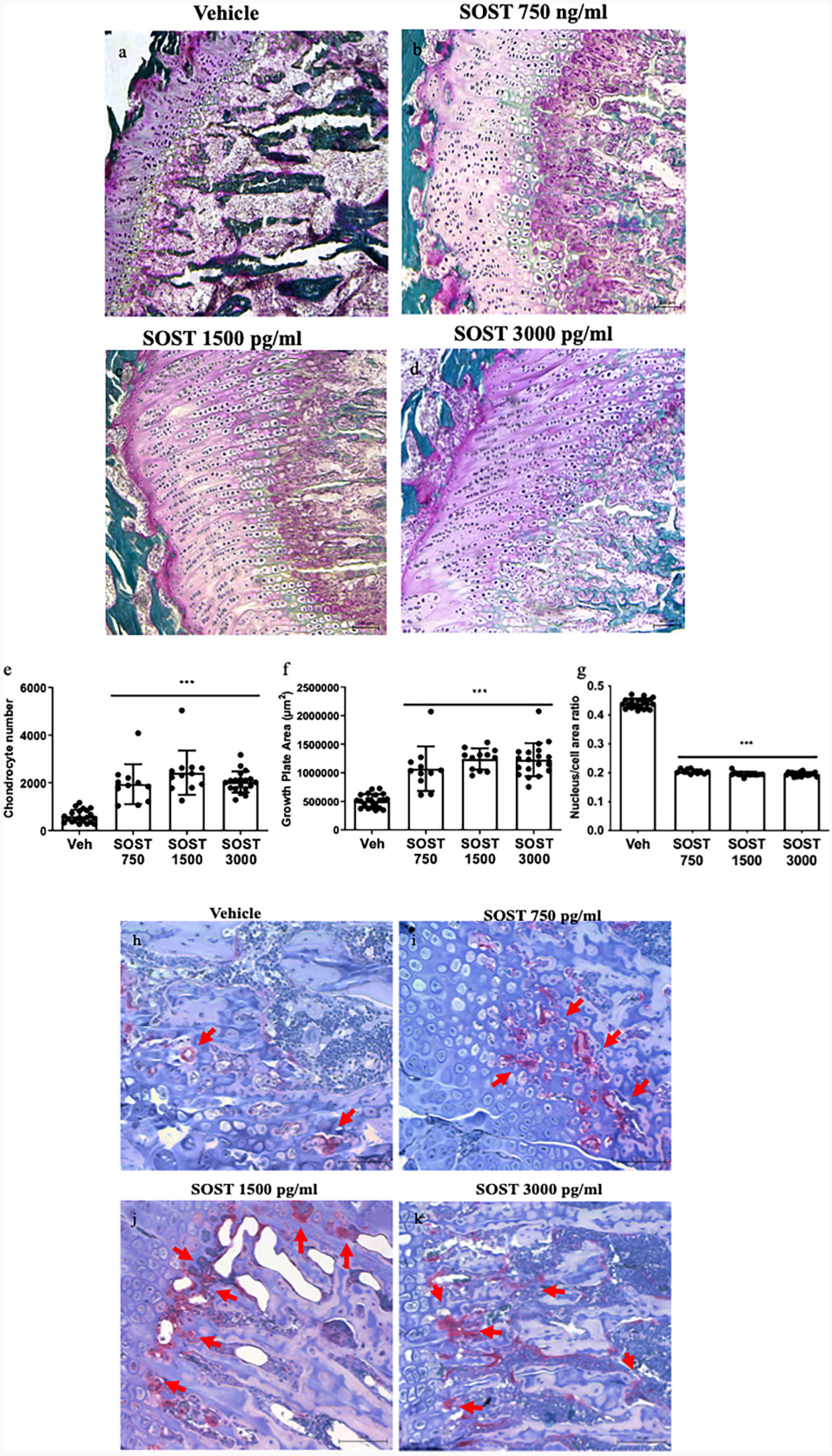

Fig. 5

The infusion of sclerostin promoted an excessive proliferation of chondrocytes in the growth plate and resorption of subchondral bone. Representative images of the growth plate of samples stained with Goldner's trichrome technique are shown: a) vehicle group, b) 750 pg/ml, c) 1,500 pg/ml, and d) 3,000 pg/ml of sclerostin (n = 5 animals per group). Figure 10× magnification. Scale bar: 100 µm. e) The number of chondrocytes and f) the growth plate area were increased with all doses of recombinant sclerostin. g) The nucleus/area ratio of the chondrocytes was significantly decreased, suggesting the presence of hypertrophic chondrocytes that became larger after sclerostin administration. The number of chondrocytes, growth plate area, and nucleus-to-area ratio were quantified by counting cells in three different fields of the bone per rat. Tartrate-resistant acid phosphatase (TRAP) staining was performed to evaluate the resorptive activity in the subchondral bone. Compared with h) the vehicle group, the number of osteoclasts in the subchondral bone, identified by their red staining (red arrows) and the presence of two or more nuclei, was significantly increased following the administration of recombinant sclerostin at doses of i) 750, j) 1,500, and k) 3,000 pg/ml (n = 5 animals per group). Figure 200× magnification. Scale bar: 100 µm.

any of the doses of sclerostin assayed, as well as statistical differences between the different concentrations of sclerostin administered.

Sclerostin administration did not affect bone mineralization

Bone mineralization was quantified by measuring the intensity of green fluorescence from calcein staining. While there was a trend toward reduced mineralization, the difference between the vehicle group and sclerostin-treated animals was not statistically significant. Supplementary Figure d presents a representative image from each experimental group and cortical mineralization quantification. Additionally, double calcein-labelled bands were observed in the cortical bone, suggesting a potential process of cortical bone trabecularization.

High levels of sclerostin produced changes in mineral metabolism parameters

Rats receiving the infusion of sclerostin had a significant increase in the urinary excretion of calcium, phosphate, and the concentration of CTx (Table I). These findings may reflect the high bone turnover with increased bone resorption and the subsequent bone loss induced by sclerostin infusion. Serum levels of calcium and phosphate were similar in the controls and the rats receiving sclerostin. Table I also shows that in the rats receiving sclerostin, the plasma levels of intact-FGF23 were increased and the PTH was reduced compared with the vehicle group. The increase in intact FGF23 levels may promote the urinary excretion of phosphate to compensate for the excessive efflux of phosphate from the bone to the extracellular space, thus preventing an elevation of serum phosphate. Notably, there was a significant decrease in intact PTH levels in rats receiving sclerostin, which suggests an inhibition of the PTH secretion by the excess of calcium released from bone.

Discussion

The results of the present study show that the administration of high concentrations of recombinant sclerostin produced significant changes in bone structure. The trabecular bone showed a substantial increase in bone turnover, with high bone resorption and a marked bone loss. Cortical bone was reduced, along with a TRAP-positive staining in some osteocytes and periosteum. In addition, a higher number of positive TRAP cells was observed around the subchondral bone of sclerostin-treated groups. It was also interesting to observe that the administration of sclerostin notably increased the number of chondrocytes and the total area of the growth plate. These bone changes were accompanied by significant alterations in parameters of mineral metabolism, including excessive urine excretion of calcium and phosphorus and elevated levels of both intact and c-terminal FGF23, with a significant reduction in the concentration of plasma PTH. In vitro, sclerostin increased osteoclastogenesis of bone marrow stem cells, determined by a high expression of cathepsin K and elevated TRAP staining.

Research involving low or null levels of sclerostin, as well as patients with van Buchem disease, exhibit significant increases in the growth of cortical bone together with reductions in calciuria. By contrast, studies examining the effects of high levels of sclerostin are scarce. Kogawa et al[13] conducted in vitro experiments that revealed the induction of osteoclastic characteristics and increased expression of carbonic anhydrase 2, TRAP, and cathepsin K, as well as a decrease in intracellular pH in cultured osteocytes upon exposure to recombinant sclerostin. Moreover, in SOST transgenic mice, a significant increase in the mean area of osteocyte lacunae within the cortical bone, compared to their wild-type littermates, was observed. The impact of elevated sclerostin on calcium release was also assessed ex vivo by Kogawa et al,[14] using bovine trabecular bone cores subjected to dynamic loading. Sclerostin treatment induced a marked increase in the ionized calcium concentration in the perfusate and the release of beta-CTx, a marker of bone resorption, concomitant with an increased average size of osteocyte lacunae. These results strongly suggest the existence of osteocytic osteolysis, providing a possible explanation for the elevated calciuria observed in our animal model. The findings by both works from Kogawa et al[13,14] align with our findings, given that positive TRAP staining was detected in some osteocytes within the cortical bone. Furthermore, the trabecularization of cortical bone with the loss of trabecular bone could also explain the excessive release of phosphate and, particularly, calcium. We do not know whether the effect of sclerostin on osteoclasts, as demonstrated in this study, also occurs in other pathologies. It is well established that factors such as inflammation,[15,16] arthroplasties,[17] and periprosthetic joint infections[18] can markedly alter bone resorption. Whether changes in sclerostin levels occur during these processes, or if sclerostin directly regulates the expression of genes related to osteoporosis, as shown in a recent study,[19] remains to be investigated.

Interestingly, another study by Zhang et al[20] using the φC31 integrase demonstrated that SOST overexpression for six weeks significantly reduced trabecular volume in the tibiae of mice, while it had no significant effect on cortical volume. This reduction in bone volume was also observed in our experimental model of recombinant sclerostin infusion. The lack of changes of cortical bone observed by Zhang et al[20] could be attributed to differences in the bone type (tibiae vs femora), species (mice vs rats), and plasma sclerostin levels, which were lower than in our own study. Winkler et al[21] used transgenic mice expressing human SOST and observed a notable loss of trabecular bone in the lumbar vertebrae with a disorganized bone architecture, thinner cortices, and presence of chondrodysplasia. However, this study did not include information on the cortical areas from long bones or the effects on calciuria and mineral metabolism-related parameters.

As mentioned, we observed a marked effect of sclerostin on the osteocytes of the femoral cortical bone. This was evidenced by positive TRAP staining and a marked loss of mineralization in the cortical bone, which was replaced by fibrous tissue. A similar effect was detected by Kogawa et al[14] in bovine trabecular bone cores devoid of bone marrow, which were subjected to daily dynamic loading with and without exposure to sclerostin. In these bovine trabecular bone samples, positive TRAP staining was observed along with an increase in ionized calcium and concentration of telopeptides in the perfusate, accompanied by an increased mean size of osteocyte lacunae, all indicative of osteocytic osteolysis.

It has been documented that serum sclerostin levels increase with ageing,[22,23] and in pathologies such as CKD,[24]

Table I. Parameters of mineral metabolism determined in plasma and urine in the experimental groups. All data are shown as mean (SD).

Parameter	Vehicle	SOST		
		750 pg/ml	**1,500 pg/ml**	**3,000 pg/ml**
Urine Ca/Cr, mg/mg	0.04 (0.02)	0.10 (0.02)†	0.36 (0.24)†	0.20 (0.06)§
Urine P/Cr, mg/mg	2.58 (0.33)	3.51 (0.32)‡	5.99 (2.70)†	3.84 (0.64)‡
Urine CTx, ng/ml	99 (32.9)	178 (49.1)*	419 (219.3)*	173 (55.6)*
Plasma Ca, mg/dl	8.60 (1.35)	8.51 (1.78)	9.22 (1.46)	8.22 (1.11)
Plasma P, mg/dl	5.45 (1.04)	5.45 (1.59)	5.43 (1.55)	5.69 (0.54)
Plasma Cr, mg/dl	0.68 (0.15)	0.64 (0.08)	0.74 (0.12)	0.58 (0.16)
iFGF23, pg/ml	281 (94)	455 (42)‡	405 (159)*	436 (146)†
cFGF23, pg/ml	293 (129)	427 (165)*	498 (278)*	523 (286)*
PTH, pg/ml	155 (68)	97 (41)*	101 (35)‡	95 (32)*

All p-values were calculated with independent-samples *t*-test.
*p < 0.05 vs control.
†p < 0.01 vs control.
‡p < 0.001 vs control.
§p < 0.0001 vs control.
Ca, calcium; cFGF23, c-terminal FGF23; Cr, creatinine; CTx, C-terminal telopeptide of type I collagen; iFGF23, intact FGF23; P, phosphorus; PTH, parathyroid hormone; SOST, sclerostin.

since these are associated with a decrease in osteoblastic activity. However, in our study, the administration of sclerostin produced an increase in the number of osteoblasts in the trabecular bone. It is known that osteoclasts are a source of bone formation-stimulating factors. In fact, the term "osteoclast-osteoblast coupling" refers to the pro-osteogenic effect induced by osteoclasts after bone resorption.[25] The secretion of soluble factors by osteoclasts, such as sphingosine 1 phosphate (S1P), semaphorin 4D (Sema 4D), collagen triple helix repeat containing 1 (CTHRC1), complement component C (C3), and Wnt family member 10B (Wnt10B), stimulate osteoblast formation.[26] Furthermore, Weivoda et al[27] demonstrated that the increased expression of leukaemia inhibitory factor (LIF), cellular repressor of E1A stimulated genes 2 (CREG2), cystatin 3 (CST3), collagen and calcium binding EGF domains (CCBE1), and dipeptidyl peptidase-4 (DPP4) by osteoclasts promotes the formation of osteoblasts. More specifically, they observed that in 52 postmenopausal women, CTx correlated significantly with serum markers of bone formation, P1NP, and osteocalcin. The decrease in CTx after denosumab treatment was a coupling-related decrease in bone formation markers (P1NP and OCN).[27] In our study, the intense osteoclastic activity induced by high levels of sclerostin resulted in increased CTx production (Table I), which could contribute to the higher number of osteoblasts observed preventing bone destruction.

There are other studies that observed an increased bone formation associated with high levels of sclerostin. A study involving 572 postmenopausal women found a positive correlation between serum sclerostin and spine and total hip BMD.[28] Additionally, Szulc et al[29] showed in 1,134 men aged 20 to 87 years that serum sclerostin levels were positively associated with better bone microarchitectural parameters, mainly trabecular architecture.

Nevertheless, the bone effects of sclerostin should be understood, taking into account the concept of the basic multicellular unit (BMU), a structure that comprises osteoclasts, osteoblasts, osteocytes, bone lining cells, osteomacs, and the capillary blood supply, regulating bone remodelling.[30] As shown by our study and others, sclerostin reduces bone formation by decreasing the activity of osteoblasts in a process mediated by inhibition of the Wnt/β-catenin pathway.[31] Bone lining cells are quiescent cells on bone surfaces that may be converted into active osteoblasts in the absence of sclerostin.[32] Accordingly, as evidenced by our study and others, the administration of sclerostin promotes bone resorption and osteoclastogenesis.[33] Osteomacs are resident macrophages present in bone tissue. Even though, to our knowledge, the precise effect of the interaction between sclerostin and osteomacs has not been investigated, it is known that these cells play a role in bone homeostasis by regulating osteoblast function.[34] In this regard, Power et al[35] investigated the effects of sclerostin at the level of the BMU in the proximal femur of patients with a hip fracture or osteoarthritis. The expression of sclerostin in osteocytes was inversely correlated with that of alkaline phosphatase, a marker of bone formation, within the BMU.

Furthermore, it is interesting to consider that in our study, the increase in the number of osteoblasts and bone turnover induced by sclerostin was independent of PTH levels, given that plasma PTH significantly decreased in plasma after sclerostin administration. With regard to the relationship between PTH and sclerostin, it has been reported that PTH inhibits sclerostin production,[5] although it is not known whether high sclerostin levels might reduce PTH secretion independent of calcium.

The role of sclerostin in the growth plate is also not well known. In human long bones, the Wnt/β-catenin pathway exerts differential influences on chondrogenic cells.

Initially, the Wnt/β-catenin pathway inhibits chondrogenic cell differentiation; however, once the chondrogenic differentiation has been initiated, Wnt/β-catenin pathway activation enhances differentiation, thus expediting the maturation of chondrocytes.[36,37] The expression of sclerostin has been well documented in hypertrophic chondrocytes located within the mineralized area of the human growth plate.[38] The significance of sclerostin in these cells appears to be linked to the ultimate maturation and mineralization of hypertrophic chondrocytes. Our experimental findings clearly demonstrate that elevated sclerostin levels result in an augmented number of hypertrophic chondrocytes and a correspondingly expanded growth plate area, likely attributable to the inhibition of the typical chondrocyte differentiation process.

Finally, it is important to note that in some experimental models where marked changes in bone structure are observed, such as osteoporosis or CKD, it can be challenging to distinguish the effects of sclerostin from those exerted by other inhibitors of the Wnt signalling pathway, such as secreted frizzled-related proteins (SFRPs) and Dkk1,[39] or from proteins similar to sclerostin, like Sostdc-1, a member of the sclerostin family expressed in bone and other tissues,[40] which may exert similar effects. It should be emphasized that our study, conducted on healthy rats, provides information specifically related to elevations in recombinant sclerostin. Therefore, the conclusions can be exclusively attributed to changes in sclerostin levels, without any interference from these other factors or the presence of concomitant pathological conditions.

This study reveals, for the first time, that elevated sclerostin levels also promote changes in mineral metabolism parameters such as urinary excretion of calcium and phosphate, which is associated with high FGF23 and low PTH. Notably, the excessive calcium and phosphate excretion resulting from intense bone resorption and high osteoclast activity is striking. It seems reasonable to speculate that the observed increase in FGF23 levels might be related to the need to enhance phosphate excretion and prevent accumulation of extracellular phosphate. These findings are consistent with those presented by Ryan et al,[41] who observed that sclerostin knockout mice exhibited reduced calcium and phosphate excretion, along with decreased intact FGF23 levels and increased plasma phosphate levels.

Intriguingly, it has been observed that in patients with X-linked hypophosphatemia (XLH) where plasma levels of FGF23 are increased and skeletal mineralization is reduced, there are elevated levels of sclerostin. Accordingly, Hyp mice, which mimic XLH pathology, also exhibit high sclerostin levels. Carpenter and Ross[42] administered anti-sclerostin antibodies to Hyp mice and observed that FGF23 levels decreased, serum phosphate increased, and cortical bone area and BV/TV also increased. In vitro, sclerostin directly stimulates the expression of FGF23 as well as GALNT3, the protein that allows the glycosylation of FGF23 and prevents its cleavage.[43] It has been documented that vitamin D stimulates the expression of sclerostin in the bone. In fact, elements responsive to vitamin D have been identified in the SOST promoter.[44] However, the effect of sclerostin on the production of vitamin D is still unknown.

Our results underscore the connection between sclerostin and other parameters of mineral metabolism such as calcium, phosphorus, PTH, and FGF23, suggesting an interplay that should be incorporated into the context of mineral metabolism-associated changes or secondary hyperparathyroidism.

Patients with advanced stages of CKD also exhibit high sclerostin levels and specific alterations of bone, in a condition known as CKD-mineral bone disease (CKD-MBD).[45,46] Beyond the PTH/sclerostin ratio,[7] the influence of elevated sclerostin levels on bone turnover in CKD-MBD has not been thoroughly examined, and our results indicate a noteworthy contribution.

This study has certain limitations. First, our work only involved male rats in order to avoid the impact of oestrogen on sclerostin, as evidenced both at the circulating[47] and bone level.[48] In this respect, further studies should be carried out in female animals to clarify whether differential effects of sclerostin might be found according to sex. On the other hand, it is noteworthy that no significant differences were observed among the various doses of sclerostin evaluated. Our research aimed to examine the effect of high sclerostin in conditions similar to those found in experimental models of CKD, such as the 5/6 nephrectomy model.[49] However, we acknowledge that, under normal renal function conditions, any of these doses are above the levels to which sclerostin typically responds. The absence of significant differences between the doses of sclerostin on most analyzed parameters may be attributed to the achievement of a maximal effect.

In conclusion, the results of this study shed light on the physiological effects of sclerostin and help us to understand its relationship with bone turnover and the associated changes in mineral metabolism. The absence of sclerostin results in increased cortical bone and a decrease in the excretion of calcium, phosphorus, and FGF23. By contrast, an increase in sclerostin leads to a decrease in both cortical and trabecular bone due to an increase in bone resorption, which is associated with elevated FGF23 and increased urinary excretion of calcium and phosphorus. Given the resorptive effect of sclerostin, it may be reasonable to think that the increased levels of sclerostin observed in CKD might contribute to the alterations in bone and mineral metabolism that characterize renal dysfunction. Nevertheless, further specific studies are needed to confirm the exact role of sclerostin in CKD-MBD.

Supplementary material

Additional information on the bone effects of high doses of recombinant sclerostin, as well as details of the femur image analysis performed using 3D Slicer software.

References

1. **Tanaka S**, **Matsumoto T**. Sclerostin: from bench to bedside. *J Bone Miner Metab*. 2021;39(3):332–340.
2. **Sebastian A**, **Loots GG**. Genetics of SOST/SOST in sclerosteosis and van Buchem disease animal models. *Metabolism*. 2018;80:38–47.
3. **Lima F**, **Monier-Faugere M-C**, **Mawad H**, **David V**, **Malluche HH**. FGF-23 and sclerostin in serum and bone of CKD patients. *Clin Nephrol*. 2023;99(5):209–218.
4. **Zeng S**, **Slowinski T**, **Pommer W**, **et al**. Sclerostin is an independent risk factor for all-cause mortality in kidney transplant recipients. *Clin Exp Nephrol*. 2020;24(12):1177–1183.
5. **Bellido T**, **Ali AA**, **Gubrij I**, **et al**. Chronic elevation of parathyroid hormone in mice reduces expression of sclerostin by osteocytes: a novel

mechanism for hormonal control of osteoblastogenesis. *Endocrinology*. 2005;146(11):4577–4583.
6. **Saidak Z**, **Le Henaff C**, **Azzi S**, **Marty C**, **Marie PJ**. Low-dose PTH increases osteoblast activity via decreased Mef2c/Sost in senescent osteopenic mice. *J Endocrinol*. 2014;223(1):25–33.
7. **Pereira L**, **Magalhães J**, **Mendonça L**, **et al**. Evaluation of renal osteodystrophy and serum bone-related biomarkers in a peritoneal dialysis population. *J Bone Miner Res*. 2022;37(9):1689–1699.
8. **National Society for Medical Research (NSMR)**. *Guide for the Care and Use of Laboratory Animals*. Eighth ed. Washington, DC: The National Academies Press, 2011.
9. **Dempster DW**, **Compston JE**, **Drezner MK**, **et al**. Standardized nomenclature, symbols, and units for bone histomorphometry: a 2012 update of the report of the ASBMR Histomorphometry Nomenclature Committee. *J Bone Miner Res*. 2013;28(1):2–17.
10. **Fedorov A**, **Beichel R**, **Kalpathy-Cramer J**, **et al**. 3D Slicer as an image computing platform for the Quantitative Imaging Network. *Magn Reson Imaging*. 2012;30(9):1323–1341.
11. **Chomczynski P**, **Sacchi N**. Single-step method of RNA isolation by acid guanidinium thiocyanate-phenol-chloroform extraction. *Anal Biochem*. 1987;162(1):156–159.
12. **Kameo Y**, **Sakano N**, **Adachi T**. Theoretical concept of cortical to cancellous bone transformation. *Bone Rep*. 2020;12:100260.
13. **Kogawa M**, **Wijenayaka AR**, **Ormsby RT**, **et al**. Sclerostin regulates release of bone mineral by osteocytes by induction of carbonic anhydrase 2. *J Bone Miner Res*. 2013;28(12):2436–2448.
14. **Kogawa M**, **Khalid KA**, **Wijenayaka AR**, **et al**. Recombinant sclerostin antagonizes effects of ex vivo mechanical loading in trabecular bone and increases osteocyte lacunar size. *Am J Physiol Cell Physiol*. 2018; 314(1):C53–C61.
15. **Dai Z**, **Chen Y**, **He E**, **et al**. Interleukin-19 promotes bone resorption by suppressing osteoprotegerin expression in BMSCs in a lipopolysaccharide-induced bone loss mouse model. *Bone Joint Res*. 2023;12(11):691–701.
16. **Toya M**, **Kushioka J**, **Shen H**, **et al**. Sex differences of NF-κB-targeted therapy for mitigating osteoporosis associated with chronic inflammation of bone. *Bone Joint Res*. 2024;13(1):28–39.
17. **Giannicola G**, **Amura A**, **Sessa P**, **Prigent S**, **Cinotti G**. Assessment of progression and clinical relevance of stress-shielding around press-fit radial head arthroplasty. *Bone Joint J*. 2023;105-B(8):905–911.
18. **Hinz N**, **Butscheidt S**, **Jandl NM**, **et al**. Increased local bone turnover in patients with chronic periprosthetic joint infection. *Bone Joint Res*. 2023;12(10):644–653.
19. **Jia Y**, **Qi X**, **Ma M**, **et al**. Integrating genome-wide association study with regulatory SNP annotations identified novel candidate genes for osteoporosis. *Bone Joint Res*. 2023;12(2):147–154.
20. **Zhang D**, **Park BM**, **Kang M**, **et al**. The systemic effects of sclerostin overexpression using ΦC31 integrase in mice. *Biochem Biophys Res Commun*. 2016;472(3):471–476.
21. **Winkler DG**, **Sutherland MK**, **Geoghegan JC**, **et al**. Osteocyte control of bone formation via sclerostin, a novel BMP antagonist. *EMBO J*. 2003;22(23):6267–6276.
22. **Lehallier B**, **Gate D**, **Schaum N**, **et al**. Undulating changes in human plasma proteome profiles across the lifespan. *Nat Med*. 2019;25(12): 1843–1850.
23. **Ardawi M-S**, **Al-Kadi HA**, **Rouzi AA**, **Qari MH**. Determinants of serum sclerostin in healthy pre- and postmenopausal women. *J Bone Miner Res*. 2011;26(12):2812–2822.
24. **Fusaro M**, **Holden R**, **Lok C**, **et al**. Phosphate and bone fracture risk in chronic kidney disease patients. *Nephrol Dial Transplant*. 2021;36(3):405–412.
25. **Durdan MM**, **Azaria RD**, **Weivoda MM**. Novel insights into the coupling of osteoclasts and resorption to bone formation. *Semin Cell Dev Biol*. 2022;123:4–13.
26. **Kim J-M**, **Lin C**, **Stavre Z**, **Greenblatt MB**, **Shim J-H**. Osteoblast-osteoclast communication and bone homeostasis. *Cells*. 2020;9(9):2073.
27. **Weivoda MM**, **Chew CK**, **Monroe DG**, **et al**. Identification of osteoclast-osteoblast coupling factors in humans reveals links between bone and energy metabolism. *Nat Commun*. 2020;11(1):87.
28. **Garnero P**, **Sornay-Rendu E**, **Munoz F**, **Borel O**, **Chapurlat RD**. Association of serum sclerostin with bone mineral density, bone turnover, steroid and parathyroid hormones, and fracture risk in postmenopausal women: the OFELY study. *Osteoporos Int*. 2013;24(2): 489–494.
29. **Szulc P**, **Boutroy S**, **Vilayphiou N**, **et al**. Correlates of bone microarchitectural parameters and serum sclerostin levels in men: the STRAMBO study. *J Bone Miner Res*. 2013;28(8):1760–1770.
30. **Kular J**, **Tickner J**, **Chim SM**, **Xu J**. An overview of the regulation of bone remodelling at the cellular level. *Clin Biochem*. 2012;45(12):863–873.
31. **Moester MJC**, **Papapoulos SE**, **Löwik CWGM**, **van Bezooijen RL**. Sclerostin: current knowledge and future perspectives. *Calcif Tissue Int*. 2010;87(2):99–107.
32. **Kim SW**, **Lu Y**, **Williams EA**, **et al**. Sclerostin antibody administration converts bone lining cells into active osteoblasts. *J Bone Miner Res*. 2017;32(5):892–901.
33. **Wijenayaka AR**, **Kogawa M**, **Lim HP**, **Bonewald LF**, **Findlay DM**, **Atkins GJ**. Sclerostin stimulates osteocyte support of osteoclast activity by a RANKL-dependent pathway. *PLoS One*. 2011;6(10):e25900.
34. **Chang MK**, **Raggatt L-J**, **Alexander KA**, **et al**. Osteal tissue macrophages are intercalated throughout human and mouse bone lining tissues and regulate osteoblast function in vitro and in vivo. *J Immunol*. 2008;181(2):1232–1244.
35. **Power J**, **Poole KES**, **van Bezooijen R**, **et al**. Sclerostin and the regulation of bone formation: effects in hip osteoarthritis and femoral neck fracture. *J Bone Miner Res*. 2010;25(8):1867–1876.
36. **Leucht P**, **Minear S**, **Ten Berge D**, **Nusse R**, **Helms JA**. Translating insights from development into regenerative medicine: the function of Wnts in bone biology. *Semin Cell Dev Biol*. 2008;19(5):434–443.
37. **ten Dijke P**, **Krause C**, **de Gorter DJJ**, **Löwik CWGM**, **van Bezooijen RL**. Osteocyte-derived sclerostin inhibits bone formation: its role in bone morphogenetic protein and Wnt signaling. *J Bone Joint Surg Am*. 2008;90 Suppl 1-A:31–35.
38. **Weivoda MM**, **Youssef SJ**, **Oursler MJ**. Sclerostin expression and functions beyond the osteocyte. *Bone*. 2017;96:45–50.
39. **Kawano Y**, **Kypta R**. Secreted antagonists of the Wnt signalling pathway. *J Cell Sci*. 2003;116(Pt 13):2627–2634.
40. **Tong X**, **Zhu C**, **Liu L**, **et al**. Role of Sostdc1 in skeletal biology and cancer. *Front Physiol*. 2022;13:1029646.
41. **Ryan ZC**, **Ketha H**, **McNulty MS**, **et al**. Sclerostin alters serum vitamin D metabolite and fibroblast growth factor 23 concentrations and the urinary excretion of calcium. *Proc Natl Acad Sci U S A*. 2013;110(15):6199–6204.
42. **Carpenter KA**, **Ross RD**. Sclerostin antibody treatment increases bone mass and normalizes circulating phosphate levels in growing Hyp mice. *J Bone Miner Res*. 2020;35(3):596–607.
43. **Ito N**, **Prideaux M**, **Wijenayaka AR**, **et al**. Sclerostin directly stimulates osteocyte synthesis of fibroblast growth factor-23. *Calcif Tissue Int*. 2021;109(1):66–76.
44. **Wijenayaka AR**, **Yang D**, **Prideaux M**, **et al**. 1α,25-dihydroxyvitamin D3 stimulates human SOST gene expression and sclerostin secretion. *Mol Cell Endocrinol*. 2015;413:157–167.
45. **De Maré A**, **Maudsley S**, **Azmi A**, **et al**. Sclerostin as regulatory molecule in vascular media calcification and the bone-vascular axis. *Toxins (Basel)*. 2019;11(7):428.
46. **Miller PD**. Chronic kidney disease and the skeleton. *Bone Res*. 2014;2: 14044.
47. **Mirza FS**, **Padhi ID**, **Raisz LG**, **Lorenzo JA**. Serum sclerostin levels negatively correlate with parathyroid hormone levels and free estrogen index in postmenopausal women. *J Clin Endocrinol Metab*. 2010;95(4): 1991–1997.
48. **Fujita K**, **Roforth MM**, **Demaray S**, **et al**. Effects of estrogen on bone mRNA levels of sclerostin and other genes relevant to bone metabolism in postmenopausal women. *J Clin Endocrinol Metab*. 2014;99(1):E81–8.
49. **Bisson SK**, **Ung RV**, **Picard S**, **et al**. High calcium, phosphate and calcitriol supplementation leads to an osteocyte-like phenotype in calcified vessels and bone mineralisation defect in uremic rats. *J Bone Miner Metab*. 2019;37(2):212–223.

Author information

M. E. Rodríguez-Ortiz, DVM, PhD, Researcher
C. Rodelo-Haad, MD, PhD, Researcher
M. Rodríguez, MD, PhD, Researcher
J. R. Muñoz-Castañeda, BSc, PhD, Researcher
Nephrology Service, Reina Sofia University Hospital, Maimonides Institute for Research in Biomedicine of Cordoba (IMIBIC), University of Cordoba, Córdoba, Spain; Health Results-Oriented Cooperative Research Network RICORS2040 (Kidney Disease), Institute of Health Carlos III, Madrid, Spain.

J. M. Díaz-Tocados, PhD, Researcher, Health Results-Oriented Cooperative Research Network RICORS2040 (Kidney Disease), Institute of Health Carlos III, Madrid, Spain; Vascular and Renal Translational Research Group, Biomedical Research Institute of Lleida, Dr. Pifarré Foundation (IRBLleida), Lleida, Spain.

A. I. Torralbo, Technician degree, Researcher
K. Valdés-Díaz, MD, Researcher
A. Rivas-Domínguez, BSc, Researcher
F. Guerrero, DVM, PhD, Researcher
I. Reina-Alfonso, BSc, Researcher
Maimonides Biomedical Research Institute of Cordoba (IMIBIC), University Hospital Reina Sofia, University of Cordoba, Córdoba, Spain.

M. Naves-Díaz, BSc, PhD, Researcher
C. Alonso-Montes, BSc, PhD, Researcher
Health Results-Oriented Cooperative Research Network RICORS2040 (Kidney Disease), Institute of Health Carlos III, Madrid, Spain; Bone and Mineral Research Unit, Hospital Universitario Central de Asturias, Instituto de Investigación Sanitaria del Principado de Asturias (ISPA), Oviedo, Spain.

Author contributions

M. E. Rodríguez-Ortiz: Investigation, Methodology, Validation, Formal analysis, Writing – original draft, .
J. M. Díaz-Tocados: Investigation, Methodology, Validation, Formal analysis, Writing – original draft.
A. I. Torralbo: Investigation, Methodology, Validation.
K. Valdés-Díaz: Investigation, Methodology, Validation.
A. Rivas-Domínguez: Investigation, Methodology, Validation.
F. Guerrero: Investigation, Methodology, Validation, Formal analysis, Writing – original draft.
I. Reina-Alfonso: Investigation, Methodology, Validation.
M. Naves-Díaz: Methodology.
C. Alonso-Montes: Methodology.
C. Rodelo-Haad: Formal analysis, Writing – original draft.
M. Rodríguez: Formal analysis, Writing – original draft, .
J. R. Muñoz-Castañeda: Formal analysis, Writing – original draft.

M. Rodríguez and J. R. Muñoz-Castañeda contributed equally to this work.

Funding statement

The authors disclose receipt of the following financial or material support for the research, authorship, and/or publication of this article: grant PI17/01010 funded by Instituto de Salud Carlos III (ISCIII) co-financed with European Funds (FEDER); grant PY20_00773 from Consejería de Transformación Económica, Industria, Conocimiento y Universidades, Junta de Andalucía; and grants PI-0169-2020 and PI-0071-2021 from Consejería de Salud y Consumo, Junta de Andalucía, as reported by M. Rodríguez and J. R. Muñoz-Castañeda. Grant PI21/0654 funded by ISCIII and co-funded by the European Union, as reported by C. Rodelo-Haad and J.R. Muñoz-Castañeda. This research was also funded by: Fondo Europeo de Desarrollo Regional (FEDER), Plan de Ciencia, Tecnología e Innovación 2018-2022 of the Principado de Asturias, grant number IDI/2021/000080; and Instituto de Salud Carlos III, RICORS2040 (Kidney Disease), grant numbers RD21/0005/0008, as reported by M. Naves-Díaz and C. Alonso-Montes. Mariano Rodriguez is a member of European Uremic Toxin Group of the ESAO (EUTOX) and principal investigator of the grant RD21/0005/0019. Mariano Rodriguez is a member of the Cost action PerMedik (CA21165). Grant PI-0169-2020 was also reported by C. Rodelo-Haad. Funding sources were not involved in the conduct of the research or the preparation of this article.

ICMJE COI statement

M. Rodríguez and J. R. Muñoz-Castañeda report: grant PI17/01010 funded by Instituto de Salud Carlos III (ISCIII) co-financed with European Funds (FEDER); grant PY20_00773 from Consejería de Transformación Económica, Industria, Conocimiento y Universidades, Junta de Andalucía; and grants PI-0169-2020 and PI-0071-2021 from Consejería de Salud y Consumo, Junta de Andalucía, all related to this study. C. Rodelo-Haad reports: grant PI21/0654 funded by ISCIII and co-funded by the European Union, related to this study; and B Action from Junta de Andalucia for the contract of clinician researchers, not related to this study. M. Naves-Díaz and C. Alonso-Montes report funding from: Fondo Europeo de Desarrollo Regional (FEDER), Plan de Ciencia, Tecnología e Innovación 2018-2022 of the Principado de Asturias, grant number IDI/2021/000080; and Instituto de Salud Carlos III, RICORS2040 (Kidney Disease), grant numbers RD21/0005/0008, RD21/0005/0019, related to this study. Grants PI-0169-2020 and RICORS2040 were also reported by C. Rodelo-Haad. If there are other authors, they declare that they have no known competing financial interests or personal relationships that could have appeared to influence the results reported in this paper.

Data sharing

The data that support the findings for this study are available to other researchers from the corresponding author upon reasonable request.

Acknowledgements

IMIBIC Nephrology Group

Rodrigo López-Baltanas, Daniel Jurado-Montoya, Javier Barba, Andrés Carmona, Teresa Obrero, Julio M. Martínez-Moreno, Raquel M. García-Sáez, M. Victoria Pendón-Ruiz de Mier.

We thank the members of the IMIBIC Nephrology Group for their participation in this work. We also thank Miguel A. Rodriguez, from the Maimonides Institute for Biomedical Research of Cordoba Facility of Preclinical Image, for the acquisition and scanning of bones. J. R. Muñoz-Castañeda is a senior researcher supported by the Nicolás Monardes Programme, Consejería de Salud-Servicio Andaluz de Salud (Junta de Andalucía). M. E. Rodriguez-Ortiz is supported by the Miguel Servet Program from Carlos III Health Institute (ISCIII) (CP21/00048).

During the preparation of this work, the authors used ChatGPT4 to improve English language in terms of grammar and redaction. After using this tool, the authors reviewed and edited the content as needed and take full responsibility for the content of the publication. No text editing tools or other artificial intelligence tools were used in the process of writing this article. Additionally, no recycled text from other papers was used.

Ethical review statement

Ethical approval for the animal studies was obtained from the Ethics Commitee for Animal Research of the University of Cordoba and Junta de Andalucia (file number 06/07/2018/113).

Open access funding

The authors report that they received open access funding for their manuscript from Consejería de Salud y Consumo, Junta de Andalucía (grant PI-0071-2021).